CCS Chemistry

RESEARCH ARTICLE

Received: Jan. 11, 2021 | Accepted: Mar. 16, 2021 | Published: May 3, 2021

A [Th_8Co_8] Nanocage-Based Metal–Organic Framework with Extremely Narrow Window but Flexible Nature Enabling Dual-Sieving Effect for Both Isotope and Isomer Separation

Mengjia Yin[1], Rajamani Krishna[2], Wenjing Wang[3], Daqiang Yuan[3], Yaling Fan[1], Xuefeng Feng[1], Li Wang[1] & Feng Luo[1]*

[1]*School of Chemistry, Biology and Materials Science, East China University of Technology, Nanchang 330013,* [2]*Van 't Hoff Institute for Molecular Sciences, University of Amsterdam, 1098 XH Amsterdam,* [3]*State Key Laboratory of Structural Chemistry, Fujian Institute of Research on the Structure of Matter, Chinese Academy of Sciences, Fuzhou 350002*

**Corresponding author:* ecitluofeng@163.com

Cite this: *CCS Chem.* **2022**, 4, 1016–1027
DOI: 10.31635/ccschem.021.202100789

The synthesis of nanoporous materials that display a combination of molecular sieving (MS) and quantum sieving (QS) effects is still a challenging task. In this work, we have demonstrated the synthesis of a nano-caged metal–organic framework (MOF), ECUT-8, that has a dual-sieving capability. ECUT-8 afforded H_2/D_2 isotope separation due to its extremely narrow window size (3.0 Å), resulting in QS. Further, the framework flexibility of ECUT-8 was exploited for the separation of butane and hexane isomers due to its MS effect. Other desirable features of ECUT-8 include high thermal, water, and chemical stability, making it suitable for practical application. Herein, these results open up an avenue to design the effects of coexistence of multiple sieving in one material.

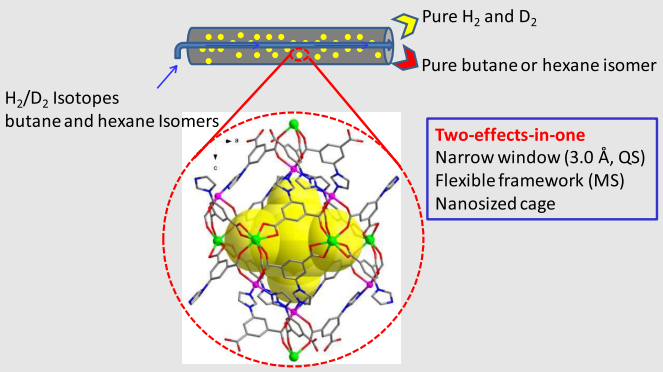

Keywords: **metal–organic framework, molecular sieving effect, quantum sieving effect, gate-opening, multiple sieving effects, isotope separation, isomer separation, thorium-based cage**

Introduction

Cages or cage-based compounds present a highly desired porous material for host–guest recognition and separation due to their internal-porosity and window-size adjustment.[1–9] Typically, the shape and size of the windows are expected to give molecular sieving (MS) effect, thereby allowing only the passage of smaller molecules, while excluding the entry of guest molecules that are larger than the window aperture. Additionally,

DOI: 10.31635/ccschem.021.202100789
Corrected Citation: *CCS Chem.* **2022**, 4, 1016–1027
Previous Citation: *CCS Chem.* **2021**, 3, 1115–1126
Link to VoR: https://doi.org/10.31635/ccschem.021.202100789

when the window size becomes small enough to distinguish the speed of diffusion of isotopes, a quantum sieving (QS) effect could be engendered.[10,11]

The separation of mixtures of molecules is an industrially important process.[12] The current mature technique for separation is based on boiling-point-differences distillation method; however, this approach requires vast capital investment and extensive energy consumption (10–15%) worldwide.[12] By contrast, the porous adsorbent-based pathway, which is relatively low-cost and energy-saving, is now receiving increasing attention.[13] Recent advances reveal that for certain unique molecular separation such as CO_2/N_2, C_2H_2/CO_2, C_2H_2/C_2H_4, C_2H_4/C_2H_6, SO_2/CO_2, and Xe/Kr, both traditional adsorbents such as zeolite and porous carbon, newly developed adsorbents such as metal–organic frameworks (MOFs), cages, hydrogen-bonded frameworks (HOFs), and covalent organic frameworks (COFs) were effective.[14–27]

Due to the closeness of physicochemical properties, separations of isotopic and isomeric mixtures pose peculiar challenges.[28,29] However, both are needed urgently in industries as they play an essential role in resolving the energy crisis. For example, the separation of deuterium (D_2) from H_2/D_2 isotope mixtures is of prime importance in the nuclear industry, and the separation of hexane isomers is of extreme importance in upgrading gasoline.[30–32]

The kinetic diameters of both H_2 and D_2 are equal to 2.9 Å. Accordingly, the H_2/D_2 separation, as suggested by theoretical and experimental results, could be achieved from a very confined system that results in different transport between H_2 and D_2 due to their differences in de Broglie wavelength.[33–40] This distinct phenomenon was defined as the QS effect.[33–40] For this QS effect to be effective, the adsorbent's efficient pore size should match precisely the kinetic diameter of H_2 and D_2. However, from the viewpoint of material synthesis, the construction of materials with ultrafine pores remains a challenging issue.

On the other hand, the isomer separation, in principle, could be achieved by exploiting the MS effects of adsorbents.[29] For example, butane isomers such as linear *n*-butane and branched *iso*-butane have respective kinetic diameters of 4.7 and 5.3 Å. In a recent report, butane isomers were separated by a microporous MOF of ZU-36-Co with the pore size ranging between 3.8 and 5.2 Å, due to MS effects in such a way that the smaller linear isomer of *n*-butane was effectively adsorbed in this MOF, whereas the bigger branched isomer of *iso*-butane was excluded beyond MOF.[41] Another example is the separation of hexane isomers whose kinetic diameters are: *n*-hexane (*n*-HEX; 4.3 Å) < 3-methylpentane (3MP; 5.0 Å) = 2-methylpentane (2MP; 5.0 Å) < 2,3-dimethylbutane (23DMB; 5.6 Å) < 2,2 dimethylbutane (22DMB; 6.2 Å), where the MS effect could be exploited using a variety of porous adsorbents such as ZIF-8 (ZIF = zeolite-like imidazole framework), $Fe_2(BDP)_3$ (BDP = 1,4-benzenedipyrazolate), Zr-bptc, and Zr-abtc.[42–47] However, the separation of monobranched isomer from dibranched isomer was still a challenging task.

As discussed in the preceding section, the separation of H_2/D_2 in light of the QS effect demands an ideal size of ~3.0 Å, whereas the separation of butane and hexane isomers relying on the MS effect needed a size >4.0 Å. Clearly, the coexistence of QS and MS effects in the same material was challenging due to the pore size requirement for an MS effect for isomer separation to be achieved, precluding the QS effect for isotope separation and vice versa. In the literature, only MIL-53 (MIL = Materials from Institut Lavoisier), a flexible MOF, has been demonstrated experimentally to exhibit the coexistence effects of both QS and MS.[37] Furthermore, given that the gate-opening phenomena are well-known in ZIFs[48–50] due to the bending or swinging of the imidazolate ring, a similar coexistence effects of QS and MS is suggested, but this has still not been confirmed experimentally.

In this work, we use an imidazolate-derivative ligand to combine 5f and 3d metal centers, resulting in a highly rare [Th_8Co_8] nanocage-based MOF (**ECUT-8**) with a 3,9-connected *ftw* topology matrix. The effective window size, down to 3.0 Å, was observed, fully meeting the QS effect requirement. As commonly observed in ZIFs, the imidazolate-derivative ligands in **ECUT-8** were flexible, leading to gate-opening and the possibility of MS effect. Both single-component adsorption tests and breakthrough experiments confirmed the isotope and isomer separation capabilities due to the coexistence effect of QS and MS.

Experimental Section

Synthesis of ECUT-8

$Co(NO_3)_2{\cdot}6H_2O$ (0.034 mmol, 10 mg), 5-(1*H*-imidazol-1-yl)isophthalic acid (0.0646 mmol, 15 mg), and $Th(NO_3)_2{\cdot}6H_2O$ (0.021 mmol, 10 mg) were dissolved in a mixture of ethanol (1 mL), *N*,*N*′-dimethylformamide (DMF; 4 mL), and concentrated HNO_3 (0.45 mL). The solution was moved into a 25 mL Teflon-lined stainless steel vessel and heated at 115 °C for 3 days, after which it was cooled down to room temperature. Red crystals were filtered and washed with 10 mL ethanol and 10 mL deionized water. The yield was 90% based on thorium (Th). Element analysis (%): Anal. Calcd for ECUT-8: C, 42.01; N, 10.49; H, 3.27. Found C, 42.08; N, 10.40; H, 3.23.

Stability test

The water stability test was carried out by immersing 100 mg **ECUT-8** samples in water at room temperature or in boiling water (100 °C) for 7 days. Then powder X-ray diffraction (PXRD) was used to trace the stability. A pH

DOI: 10.31635/ccschem.021.202100789
Corrected Citation: *CCS Chem.* **2022**, 4, 1016–1027
Previous Citation: *CCS Chem.* **2021**, 3, 1115–1126
Link to VoR: https://doi.org/10.31635/ccschem.021.202100789

stability test was performed by immersing 100 mg samples in water at pH 3.0–12 for 1 day. Then PXRD was used to trace the stability. The thermal stability test was conducted by calcining 100 mg samples in N_2 at high temperature (350 °C) for 1 day. Then PXRD was used to trace the stability.

X-ray crystallography

X-ray diffraction data of **ECUT-8** were collected at 298 K on a Bruker-Apex (II) diffractometer using graphite-monochromated MoKα radiation (λ = 0.71073 Å). Data reduction included the correction for Lorentz and polarization effects, and an applied multiscan absorption correction (SADABS). The crystal structure was solved and refined using the SHELXTL program suite. Direct methods yielded all nonhydrogen atoms, which were refined with anisotropic thermal parameters. All hydrogen atom positions were calculated geometrically and were found overlapped with their respective atoms. The SQUEEZE subroutine of the PLATON software suite (~https://www.chem.gla.ac.uk/~louis/software/platon/index.html) was used to remove the scattering from the highly disordered guest molecules. CCDC 2055060 contains the supplementary crystallographic data of **ECUT-8**. The data are available free of charge from the Cambridge Crystallographic Data Centre via www.ccdc.cam.ac.uk/data_request/cif A crystallographic summarization is shown in Supporting Information Table S1.

Results and Discussion

ECUT-8 structure

The MOF with the formula of [ThCoL$_3$] [L^{2-} = 5-(1*H*-imidazol-1-yl)isophthalate] was synthesized by the solvothermal reaction of Th(NO$_3$)$_4$, Co(NO$_3$)$_2$, and L in DMF in the presence of HNO$_3$ at 120 °C. The yield was up to 90% based on Th. Single-crystal X-ray diffraction revealed that **ECUT-8** crystallized in the rhombohedral crystal system with *R*3$_2$ space group. In the asymmetric unit, there was one crystallography-independent Th and one Co site. The Th(IV) site is coordinated by nine carboxylate oxygen atoms from six L^{2-} ligands, while the Co(II) site held a common octahedral geometry finished by three carboxylate oxygen atoms from three L^{2-} ligands and three nitrogen atoms from the other three L^{2-} ligands. Each L^{2-} ligand connects to two Th(IV) ions

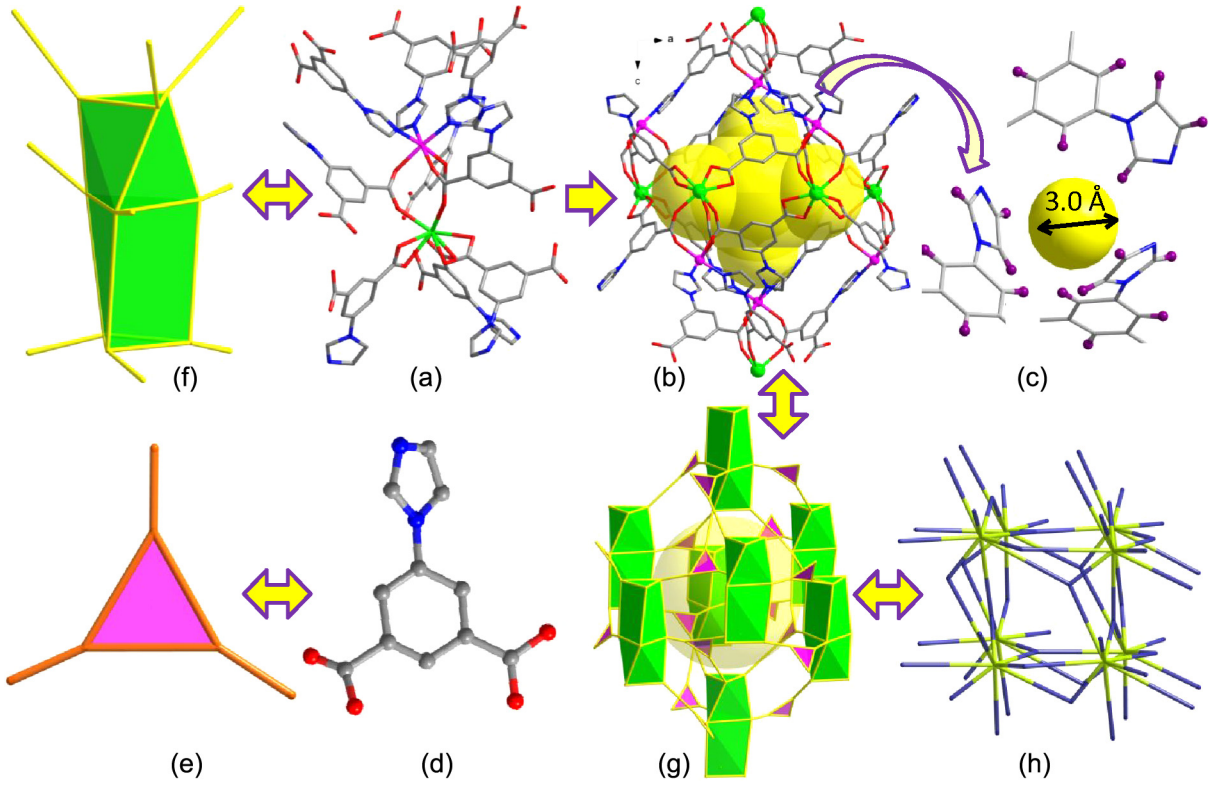

Figure 1 | *The structure of **ECUT-8**. (a) View of the ThCo dinuclear unit bridged by three L^{2-} carboxylate groups and connects to nine L^{2-} ligands. (b) View of the [Th$_8$Co$_8$] cage in a hexagonal biconical configuration with the highlighted large cavity about 0.8 nm aperture. (c) View of the narrow six-ring window (3.0 Å). (d) View of the imidazolate-derivated L^{2-} ligands. (e) The simplified three-connected triangle node. (f) The simplified nine-connected three-capped triangular prism node. (g) The simplified [Th$_8$Co$_8$] cage. (h) The overall 3,9-connected* ftw *topology matrix in **ECUT-8**.*

DOI: 10.31635/ccschem.021.202100789
Corrected Citation: *CCS Chem.* **2022**, 4, 1016–1027
Previous Citation: *CCS Chem.* **2021**, 3, 1115–1126
Link to VoR: https://doi.org/10.31635/ccschem.021.202100789

and two Co(II) ions with one carboxylate in the chelate mode and the other in the bridging mode. The secondary building unit in **ECUT-8** is the ThCo dinuclear unit, where the Th and Co center were bridged by three L^{2-} carboxylate groups (Figure 1a). The novel Th_8Co_8 nanocage, composed of eight ThCo dinuclear units in a hexagonal biconical configuration, is shown in Figure 1b. The effective aperture, excluding the van der Waals radii of atoms, is ~8.0 Å, with a great window size of only 3.0 Å (Figure 1c). A careful inspection of the window structure suggested a high degree of similarity with the narrow six-ring window (3.4 Å) in ZIF-8 (Supporting Information Figure S1).[48–50] The unique structural feature of ZIF-8 is the framework flexibility caused by the bending or swinging of the imidazolate unit, leading to an open gating and the possibility of separation due to the MS effect. Analogously, **ECUT-8**, with a comparable structural feature, is expected to exhibit similar open gating and along with the MS effect. Most importantly, the very small window (3.0 Å) in **ECUT-8** matches well with the kinetic diameter of H_2 and D_2 (2.9 Å), strongly suggesting its potential for H_2/D_2 separation via the QS effect.

Further analysis of the topology of this MOF revealed that each of the L^{2-} ligands was connected to three identical ThCo dinuclear units, while each ThCo dinuclear unit was connected to nine L^{2-} ligands. Given the connectivity of the L^{2-} ligands and ThCo dinuclear units, they were simplified as forming three-connected triangle nodes (Figures 1d and 1e) and nine-connected three-capped triangular prism nodes (Figure 1f), respectively. Subsequently, a simplified nanocage was obtained as shown in Figure 1g, rendering an overall 3,9-connected *ftw* topology matrix (Figure 1h) with the short topology symbol, $(4^26)(4^66^{27}8^3)$.[51]

ECUT-8 stability and porosity

The thermal stability of **ECUT-8** was initially investigated by thermogravimetric analysis (TGA), resulting in the loss of solvent molecules before 340 °C (Supporting Information Figure S2). Notably, this MOF displayed ultrahigh thermal and chemical stability; for example, calcining at 350 °C for 24 h, stable after immersion in water or boiling water for 7 days, as well as immersion in acidic or alkaline solution at pH 3–12 for 24 h. This was confirmed by PXRD, shown as representative photographs of the samples in Figures 2a and 2b). After methanol exchange, the activated **ECUT-8** samples were obtained by raising the temperature to 150 °C under vacuum. A type I profile of N_2 adsorption at 77 K was observed for the activated samples (Supporting Information Figure S3). The Brunauer–Emmett–Teller (BET) surface area and pore volumes were 760 m^2/g and 0.34 cm^3/g, respectively. Besides, a narrow pore size distribution at 0.76 nm was observed, consistent with the aperture (0.8 nm) of $[Th_8Co_8]$ cage.

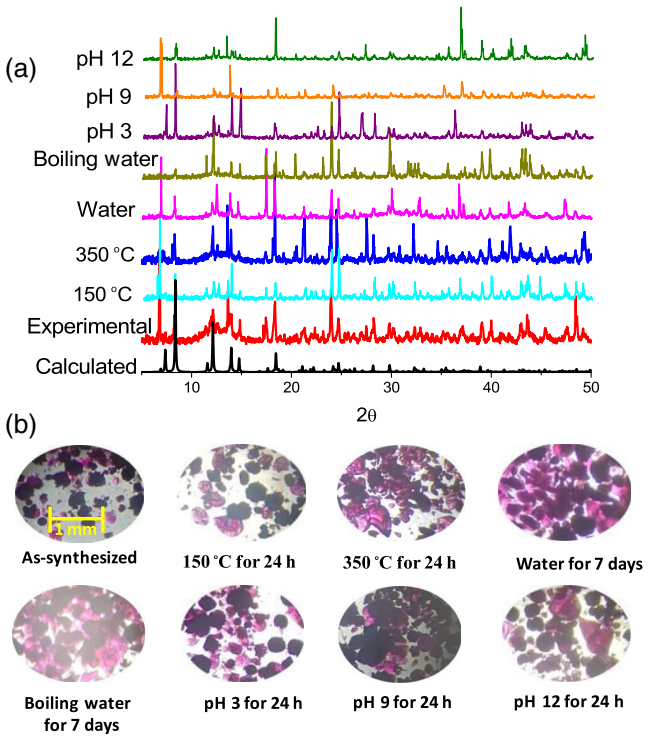

Figure 2 | *The stability test of **ECUT-8**. (a) A comparison of PXRD patterns for the calculated one from single-crystal data, the as-synthesized samples, and the samples after activation (150 °C) or calcination (350 °C), or immersing in water, or boiling water, or acidic/alkaline solution. (b) The photograph of the as-synthesized samples and the samples after activation (150 °C) or calcination (350 °C), or immersing in water, or boiling water, or acidic/alkaline solution.*

H_2/D_2 separation

Recent advances disclose that H_2/D_2 separation could be achieved through the QS effect.[33–40] Accordingly, two dominating methods emerged to obtain the QS effect, viz, designing ultramicroporous materials with windows or apertures of ~3.0 Å and constructing porous materials with open-metal sites. Additionally, a very recent discovery disclosed that flexible MOFs could be effective candidates.[37] Moreover, in a recent report, the combined QS effects were attested to be effective.[39] In the literature, both the cryogenic thermal desorption spectroscopy (TDS) measurements and breakthrough experiments have been employed to confirm the actual separation ability of porous materials. By contrast, only limited cases were investigated through breakthrough experiments to be effective, presenting a commonly used method for evaluating separation.[36]

The extremely narrow window in **ECUT-8** exactly matches with the kinetic diameter of H_2 and D_2, suggesting that it might be suitable for H_2/D_2 isotope separation. As shown in Figure 3a, **ECUT-8** enabled high D_2

DOI: 10.31635/ccschem.021.202100789
Corrected Citation: *CCS Chem.* **2022**, 4, 1016–1027
Previous Citation: *CCS Chem.* **2021**, 3, 1115–1126
Link to VoR: https://doi.org/10.31635/ccschem.021.202100789

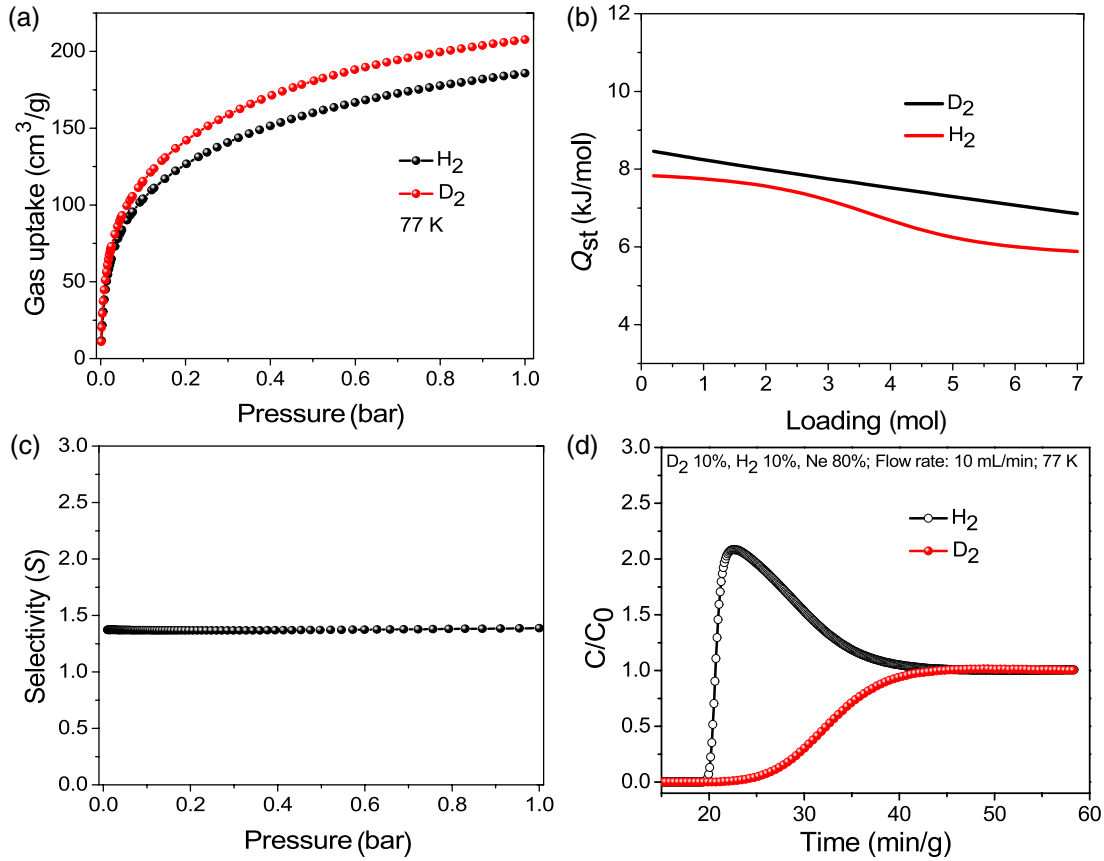

Figure 3 | *The H_2, D_2 adsorption, and separation using **ECUT-8** column. (a) The H_2 and D_2 adsorption isotherms at 77 K. (b) The Q_{st} value of D_2 and H_2 based on the adsorption data at 77 and 87 K. (c) The D_2/H_2 selectivity at 77 K. (d) The breakthrough experiments upon **ECUT-8** for D_2/H_2 separation.*

adsorption capacity up to 208 cm^3/g at 1 bar and 77 K. By contrast, H_2 uptake under the same condition was 186 cm^3/g, lower than D_2 uptake, which was ~22 cm^3/g, indicative of selective adsorption of D_2 than H_2. These results in conjunction with the narrow window (3.0 Å) obtained in **ECUT-8**, implied a strong relationship between H_2/D_2 separation and the QS effect. To evaluate the binding energy between the MOF framework and hydrogen isotopes, we further carried out calculation of adsorption enthalpies (Q_{st}) for D_2 and H_2 applying the virial equation of state, with the use of the unary adsorption isotherm data at 77 and 87 K (Supporting Information Figure S4), giving 8.4 kJ/mol for D_2, stronger than the 7.9 kJ/mol obtained for H_2 at zero coverage (Figure 3b). The selective adsorption of D_2 over H_2 was then evaluated by the ideal adsorption solution theory (IAST),[24,25] giving D_2/H_2 selectivity of 1.38 for an equimolar D_2/H_2 mixture at 77 K and 1 bar (Figure 3c). To further confirm its actual D_2/H_2 separation performance, the dynamic breakthrough experiment was performed using an **ECUT-8** column set at 77 K and 1 bar with an H_2/D_2/Ne (10/10/80, vol %) mixture. Remarkably, H_2 was first eluted through the packed column after 19 min/g, whereas the retention time for D_2 was after 23 min/g, suggesting complete D_2/H_2 separation (Figure 3d).

ECUT-8 flexibility

It is well known that ZIF series constructed from imidazolate or imidazolate-like ligands based on the local flexibility of imidazolate or imidazolate-like ligands such as bending or swinging or rotating movement. This property often enables flexible adsorption, viz, the so-called gate opening, endowing the ZIF series to effectively adsorb molecules that show bigger size than the window of ZIF materials, consequently leading to the MS separation effect.[48-50] For example, ZIF-8 displays a narrow six-ring window of ~3.4 Å and a large cage of ~11.4 Å, which is theoretically expected to separate hydrogen (2.9 Å kinetic diameter) from larger molecules like methane (3.8 Å) and nitrogen (3.6 Å). However, selective adsorption of larger molecules, as evidenced by experimental results and theoretical calculation, was observable mainly due to gate opening.[48-50] This phenomenon of flexible adsorption was also observed in MIL-53.[37] In **ECUT-8**, imidazolate-like ligands were used with a

DOI: 10.31635/ccschem.021.202100789
Corrected Citation: *CCS Chem.* **2022**, 4, 1016–1027
Previous Citation: *CCS Chem.* **2021**, 3, 1115–1126
Link to VoR: https://doi.org/10.31635/ccschem.021.202100789

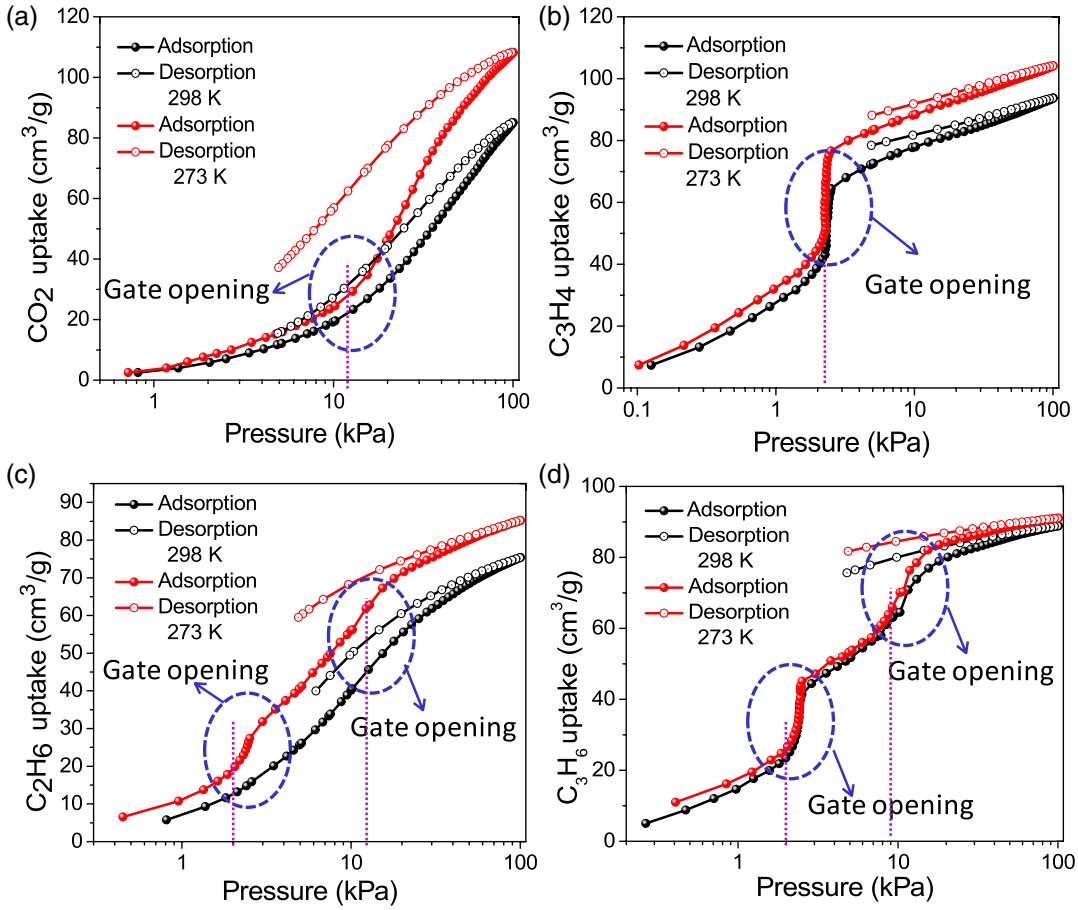

Figure 4 | *The flexibility research through CO_2, C_3H_4, C_2H_6, and C_3H_6 molecular probes with the size varying from 3.3 to 4.7 Å. (a–d) The adsorption isotherms at 298 and 273 K. The highlighted section is the step-like adsorption due to gate opening.*

six-ring narrow window analogous to ZIF-8; thus, flexible adsorption was also expected with this fabrication. In this regard, we first tested CO_2 adsorption, which showed a kinetic diameter of 3.3 Å, slightly larger than the window size (3.0 Å). As shown in Figure 4a, almost "step-shaped" adsorption and evident hysteresis were observed for CO_2 at 298 and 273 K, implying the existence of gate opening in **ECUT-8**.[50] We confirmed this gate opening phenomenon further by exploring the effective aperture size in **ECUT-8** using a series of probe molecules including C_3H_4 (4.2 Å), C_2H_6 (4.4 Å), and C_3H_6 (4.7 Å). The results are shown in Figures 4b–4d. Interestingly, in contrast to CO_2 molecules, C_3H_4 molecules afforded clearer "step-shaped" adsorption. Impressively, increasing the molecule size resulted in an observation of "two-step" gate opening for C_2H_6 (4.4 Å) and C_3H_6 (4.7 Å) molecules, where the first and second "step-shaped" transitions occurred at pressures of ~1.2 kPa and ~10 kPa, respectively. These results indicated that the flexibility of **ECUT-8** allowed the adsorption of larger molecules. For molecular sizes in the 3.3–4.2 Å range, the framework showed "one-step" adsorption profiles. To enable the passage of molecules larger than 4.2 Å, a "two-step" gate opening was necessary, and to the best of our knowledge, such gate-opening phenomenon is not observable in ZIF series.

Butane and hexane isomer separation

Separation of the linear isomer from the branched isomers is necessary for the production of high-quality commodities in the petrochemical industry. For example, enhancing the research octane number (RON) and the subsequent upgrade of gasoline.[32] For both butane and hexane isomers, their linear isomer and branched isomers showed similar physical and chemical properties, especially their comparable molecule size; thus, creating a major challenge for separation. More importantly, hexane isomer contains three components, namely, linear, monobranched, and dibranched isomers. Most porous adsorbents could separate the linear isomer from the monobranched isomer effectively; however, complete separation of the linear, monobranched, and dibranched isomers remains a challenging task.[42–47]

DOI: 10.31635/ccschem.021.202100789
Corrected Citation: *CCS Chem.* **2022**, 4, 1016–1027
Previous Citation: *CCS Chem.* **2021**, 3, 1115–1126
Link to VoR: https://doi.org/10.31635/ccschem.021.202100789

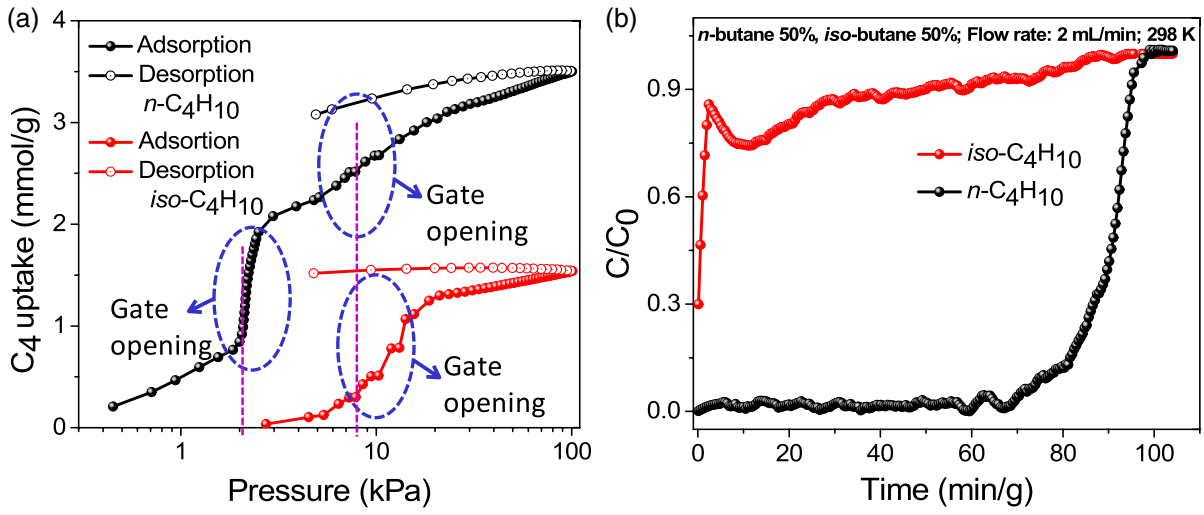

Figure 5 | *Butane separation research. (a) The adsorption isotherms of* n*-butane and* iso*-butane at 298 K. The highlighted section is the "step-shaped" gate opening. (b) The breakthrough experiments on* ***ECUT-8*** *column for* n*-butane and* iso*-butane at 298 K.*

As discussed above, the flexibility in **ECUT-8** permits it to exhibit a "two-step" gate opening effect, thereby allowing for the adsorption of large molecules. In this regard, **ECUT-8** was presumed to enable the MS effect for butane and hexane isomer. First, we tested the adsorption of butane isomers (*n*-butane/*n*-C_4H_{10} vs *iso*-butane/*iso*-C_4H_{10}), as shown in Figure 5a. The linear isomer of *n*-C_4H_{10} gave the kinetic diameter of 4.7 Å, comparable with C_3H_6. Thus, a "two-step" gate opening was expected for *n*-C_4H_{10}. Indeed, this was observed for *n*-C_4H_{10}, where the pressures for the "two-step" gate opening were ~1.2 and 6.3 kPa, respectively. The adsorption capacity of *n*-butane at 298 K and 100 kPa was as high as 3.5 mmol/g. This value exceeded that observed for most reported porous adsorbents such as ZU-36-Co (2.1 mmol/g),[41] Y-fum-fcu-MOFs (2.0 mmol/g),[52] and commercial 5A zeolite (1.3 mmol/g).[41] By contrast, a new "one-step" gate-opening profile was observed for larger molecules like *iso*-butane (5.3 Å), with the corresponding gate-opening pressure of ~6.3 kPa; thus, significantly reducing the *iso*-butane uptake to 1.2 mmol/g at 298 K and 100 kPa. These results indicated higher selective adsorption of *n*-butane over *iso*-butane due to the MS effect, resulting from the flexibility of the MOF framework.

The adsorption selectivity for equimolar *n*-butane/*iso*-butane mixtures was calculated to be 130.5 at 100 kPa and 298 K (Supporting Information Figure S5). This result

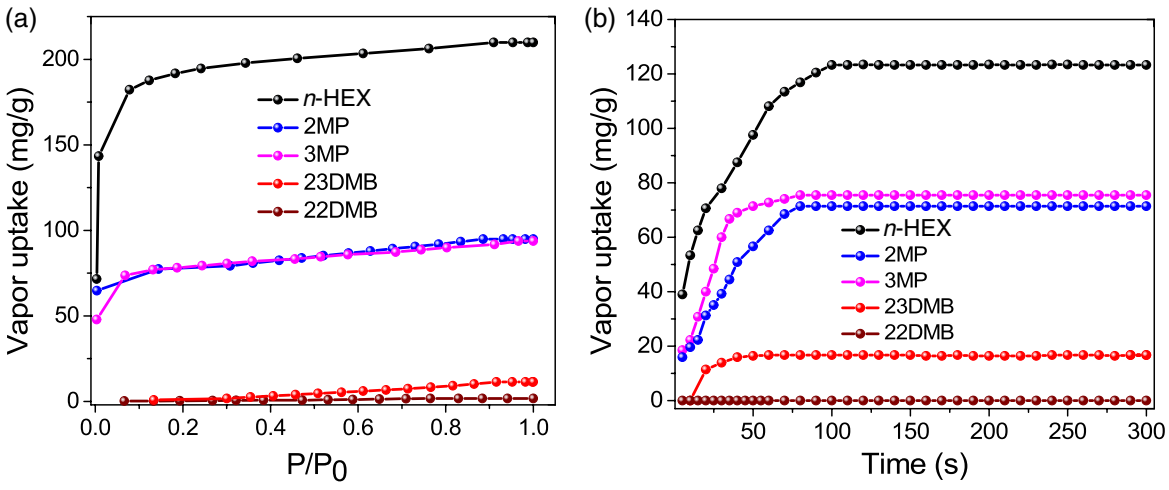

Figure 6 | *The vapor adsorption of hexane isomers upon* ***ECUT-8*** *at 298 K. (a) The adsorption isotherms of hexane isomers. (b) The adsorption kinetics of hexane isomers.*

DOI: 10.31635/ccschem.021.202100789
Corrected Citation: *CCS Chem.* **2022**, 4, 1016–1027
Previous Citation: *CCS Chem.* **2021**, 3, 1115–1126
Link to VoR: https://doi.org/10.31635/ccschem.021.202100789

implied its outstanding potential in *n*-butane/*iso*-butane separation. Further, to confirm the actual separation potential, breakthrough experiments on the **ECUT-8** column were carried out for an equimolar *n*-butane/*iso*-butane mixture at 298 K (Figure 5b). As anticipated, *iso*-butane flowed through the column almost immediately, suggesting that the *iso*-butane adsorption was excluded by **ECUT-8**, owing to the MS effect, fully consistent with the adsorption results and structural analysis. By contrast, *n*-butane was retained in the **ECUT-8** column for a very long time, up to 70 min/g. The *n*-butane adsorption capacity is as high as 3.25 mmol/g, equal to 97% of the theoretical adsorption capacity (3.35 mmol/g at 0.5 bar). This value by far exceeded that of the benchmark material of ZU-36-Co (0.89 mmol/g).[41] The productivity of pure *iso*-butane (>99.9%) was as high as 68 mL/g, also by far exceeding the benchmark material of ZU-36-Co (17.5 mL/g).[41] These results strongly suggested that **ECUT-8** is superior regarding its application in C_4 isomer separation.

As discussed above, with **ECUT-8**, the adsorption of a guest molecule with a size below 4.4 Å occurred through a "one-step" gate-opening mechanism, while the uptake of a guest molecule with a size of ~4.4–4.7 Å occurred through a "two-step" gate opening. As the size of guest molecules continued to increase, there was a significant reduction of guest molecule uptake due to the MS effect. In this regard, the flexibility in **ECUT-8** could expand its effective window aperture to 4.7 Å. However, when the sizes of guest molecules were larger than the enhanced aperture, no adsorption was guaranteed due to the MS effect. The kinetic diameter of *iso*-butane was 5.3 Å and, therefore, was excluded from the pores, as demonstrated in the breakthrough experiments in Figure 5. The linear isomers of *n*-HEX had a kinetic diameter of 4.3 Å, close to the criterion required for an occurrence of "one-step" gate opening. The monobranched isomers of 3MP and 2MP had a larger kinetic diameter of 5.0 Å, a slightly larger size than that achievable with *iso*-butane. Accordingly, due to the MS effect, a reduced uptake for monobranched isomers was expected. As for the dibranched isomers of 23DMB and 22DMB, they afforded the largest kinetic diameter in the range of 5.6 and 6.2 Å, far exceeding all tested molecule probes; thus, no adsorption due to the MS effect was expected. In this regard, a complete separation of hexane isomer was achieved.

Figure 6a presents the results of hexane vapor adsorption at 30 °C. Ultrahigh *n*-HEX adsorption capacity up to 209 mg/g was observed that exceeded most top-performing adsorbents for this task,[42–47] including Al-bttotb (151 mg/g),[46] Ca-tcpb (150 mg/g),[45] MIL-53(Fe)-$(CF_3)_2$ (32 mg/g),[44] and $Fe_2(BDP)_3$ (113 mg/g).[43] By contrast, the uptake of monobranched isomers was relatively lower, yielding 93.2 and 93.8 mg/g for 3MP and 2MP, respectively. Impressively, almost no adsorption (1.0 mg/g) and extremely low adsorption of 10.7 mg/g were observed for the dibranched isomers, 22DMB and 23DMB, respectively. These results were consistent with our expectations and suggested a potential for complete separation of a mixture of linear, monobranched, and dibranched isomers. Additionally, we performed an investigation on the adsorption kinetics of **ECUT-8**. As shown in Figure 6b, **ECUT-8** shows high *n*-HEX uptake, moderate 2MP, and 3MP uptakes, low 23DMB uptake, and no uptake of 22DMB, agreeing well with the adsorption isotherms data. These differences in adsorption kinetics also implied its potential for total separation of hexane isomers.

All investigations in the published literature used multicomponent column breakthrough measurements with hexane vapor mixtures to test the separation capability of various MOFs in the partition of hexane isomers.[42–47] From the standpoint of energy efficiency, it is preferable to carry out hexane isomer separation in the liquid phase because the boiling points of hexane isomers were above room temperature in the range of 323–341 K. Next, we confirmed the practical separation capability using a series of batch experiments with binary or ternary or quaternary mixtures in the liquid phase (Table 1 and Supporting Information Figures S6–S15). In each case, the activated **ECUT-8** samples were immersed initially in the liquid-phase mixture. Subsequently, the adsorbed

Table 1 | *A Summary of Hexane Separation Upon* ***ECUT-8***

Entry	*n*-HEX	2MP	3MP	22DMB	Product	Purity (%)	Capacity (mg/g)
1	√	√			*n*-HEX	>99.9%	150
2	√		√		*n*-HEX	>99.9%	160
3	√			√	*n*-HEX	>99.9%	130
4		√	√		3MP	>99.9%	58
5		√		√	2MP	>99.9%	38
6			√	√	3MP	>99.9%	46
7	√		√	√	*n*-HEX	>99.9%	140
8		√	√	√	3MP	>99.9%	60
9	√	√	√	√	*n*-HEX	>99.9%	110

DOI: 10.31635/ccschem.021.202100789
Corrected Citation: *CCS Chem.* **2022**, 4, 1016–1027
Previous Citation: *CCS Chem.* **2021**, 3, 1115–1126
Link to VoR: https://doi.org/10.31635/ccschem.021.202100789

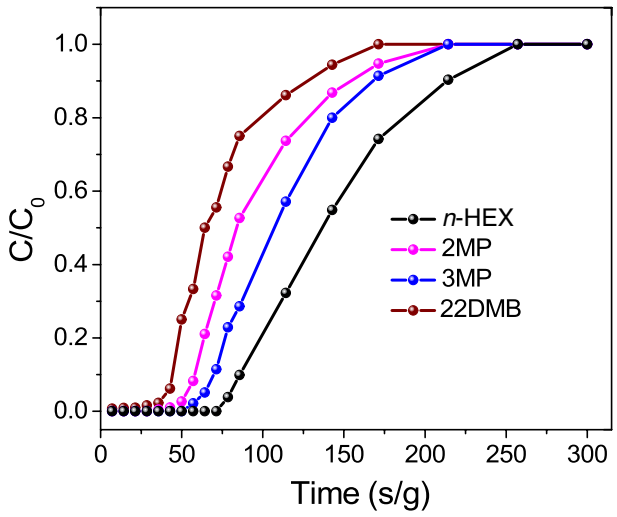

Figure 7 | *The breakthrough research of hexane isomers upon* ***ECUT-8*** *column at 298 K.*

contents were extracted using *n*-butyl acetate from the samples after drying naturally. Impressively, 100% pure linear *n*-HEX was recovered from the binary linear/mono-branched or linear/dibranched mixtures. Also, a complete separation of monobranched isomers from monobranched/dibranched mixtures was realized. Even more remarkably, 100% pure 3MP was also separated from the 2MP/3MP binary mixtures. Further, sharp separation peaks were obtained with the ternary mixtures, with 100% recovery of pure *n*-HEX from *n*-HEX/3MP/22DMB mixtures, and 100% 3MP was recovered from 3MP/2MP/22DMB mixtures. Moreover, 100% *n*-HEX was recovered from a quaternary *n*-HEX/3MP/2MP/22DMB mixture. Collectively, these results strongly suggest that the complete separation of hexane isomer with 100% pure linear or 100% monobranched product is feasible, with attractive productivity. For example, 160, 140, and 110 mg/g pure *n*-HEX were recovered from the *n*-HEX/3MP, *n*-HEX/3MP/22DMB, and *n*-HEX/3MP/2MP/22DMB mixtures, respectively, while 46 mg/g pure 3MP was

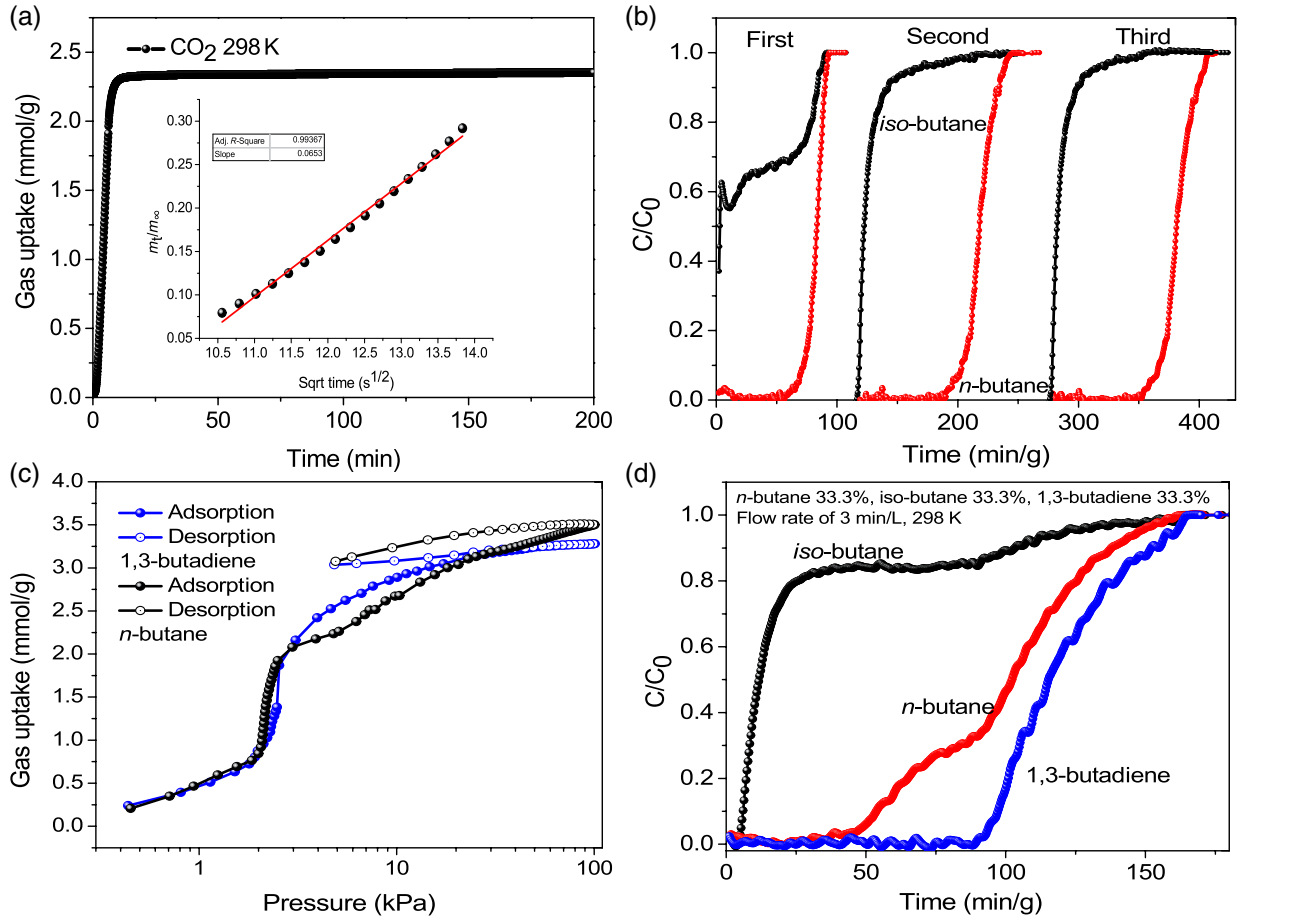

Figure 8 | *(a) The time-dependent CO_2 uptake profiles with the insert of the diffusivity calculation. (b) The recycle tests of breakthrough experiments on the separation of* n*-butane and* iso*-butane mixtures at 298 K (*n*-butane: 50%,* iso*-butane: 50%, flow rate of 2 min/L). (c) A comparison of* n*-butane and 1,3-butadiene adsorption isotherms at 298 K. (d) The breakthrough experiments on the separation of* n*-butane,* iso*-butane, and 1,3-butadiene mixtures.*

DOI: 10.31635/ccschem.021.202100789
Corrected Citation: *CCS Chem.* **2022**, 4, 1016–1027
Previous Citation: *CCS Chem.* **2021**, 3, 1115–1126
Link to VoR: https://doi.org/10.31635/ccschem.021.202100789

recovered from a 3MP/22DMB mixtures. Even with 3MP/2MP mixtures, a high 3MP recovery of 58 mg/g was realized. To further confirm the practical separation capability, we also, for the first time, carried out direct separation via multicomponent column breakthrough measurements with a four-component liquid-phase mixture (Figure 7). The results show that **ECUT-8** was capable of separating hexane isomers into individual components. 22DMB broke first from the **ECUT-8** column after 24 s/g, with the retention times for 2MP, 3MP, and *n*-HEX being 42, 58, and 72 s/g, respectively.

Diffusion, recycling, stability, and other applications of ECUT-8

The diffusivity of a gas molecule that passes through porous adsorbents is another critical factor for the separation application. For **ECUT-8**, the diffusivity was investigated using a CO_2 molecule. Figure 8a shows the time-dependent CO_2 uptake profiles, revealing a fast adsorption equilibrium within 10 min. The diffusivity was calculated to be 3.1×10^{-10} m^2/s, comparable with that observed in other porous adsorbents.[22] Besides, investigating recycling and stability properties of nanocaged MOF materials after breakthrough experiments is also crucial in determining their application in materials' separation. Thus, we investigated the recycling capability of **ECUT-8** using breakthrough experiments for the separation of *n*-butane and *iso*-butane mixture at 298 K. After three repetitions of the process, there was no apparent decrease in separation performance (Figure 8b). The maintenance of framework integrity was further confirmed by PXRD patterns obtained from the samples after completing the breakthrough experiments (Supporting Information Figure S16). Moreover, the separation of C_4 isomers was extended further to 1,3-butadiene. The adsorption isotherm of 1,3-butadiene at 298 K showed a "one-step" gate-opening profile (Figure 8c). The uptake at 298 K and 1 bar was up to 3.3 mmol/g, comparable with the uptake of *n*-butane (3.5 mmol/g), but far higher than the uptake of *iso*-butane (1.2 mmol/g). Breakthrough experiments for *n*-butane, *iso*-butane, and 1,3-butadiene mixtures at 298 K were carried out to evaluate the actual separation capacities. Interestingly, complete separation of *n*-butane, *iso*-butane, and 1,3-butadiene mixtures were observed (Figure 8d), with a breakthrough time of 4.7 min/g for *n*-butane, 44 min/g for *iso*-butane, and 90 min/g for 1,3-butadiene, respectively. The separation of 1,3-butadiene from *iso*-butane was due to the selective adsorption of 1,3-butadiene over *iso*-butane. Although **ECUT-8** showed comparable adsorption of 1,3-butadiene from *n*-butane; however, the real separation of 1,3-butadiene from *n*-butane might have resulted from the differences in the adsorption type such as "one-step" gate opening for 1,3-butadiene versus "two-step" gate opening for *n*-butane.

Conclusion

In this work, we report the synthesis, structure, and adsorption properties of a rare and highly rare 3d–5f bimetal cage-based MOF called **ECUT-8**, which exhibited a combination of QS and MS characteristics. **ECUT-8** contained a unique $[Th_8Co_8]$ nanocage with 3.0 Å windows, fulfilling the criterion to demonstrate the QS effect for H_2/D_2 separation. Additionally, due to the flexibility of imidazolate-derivative ligands observable in ZIFs, the effective aperture of **ECUT-8** was expandable, and consequently, molecules with kinetic diameters <5.6 Å could pass through the window of **ECUT-8** utilizing "one-step" or "two-step" gate-opening mechanisms. This afforded the MS property necessary for isomer separation. Breakthrough experiments have provided convincing evidence for **ECUT-8** to perform clear separations of both H_2/D_2 isotopes and butane/or hexane isomers due to the distinctive feature of coexistence of both QS and MS effects in **ECUT-8**.

Supporting Information

Supporting Information is available and includes experiments in detail, Figures S1–S16, and Table S1.

Conflict of Interest

There is no conflict of interest to report.

Preprint Acknowledgment

The research presented in this article was posted on a preprint server prior to publication in CCS Chemistry. The corresponding preprint article can be found here: https://doi.org/10.21203/rs.3.rs-99357/v1

Acknowledgments

This work was supported financially by the National Natural Science Foundations of China (nos. 21966002, 21871047, and 21861017), the Natural Science Foundation of Jiangxi Province of China (no. 20181ACB20003), and the Training Program for Academic and Technical Leaders of Major Disciplines in Jiangxi Province (no. 20194BCJ22010).

References

1. Rowland, C. A.; Lorzing, G. R.; Gosselin, E. J.; Trump, B. A.; Yap, G. P. A.; Brown, C. M.; Bloch, E. D. Methane Storage in Paddlewheel-Based Porous Coordination Cages. *J. Am. Chem. Soc.* **2018**, *140*, 11153–11157.
2. Liu, Y.; Zhao, W.; Chen, C.-H.; Flood, A. H. Chloride Capture Using a C-H Hydrogen-Bonding Cage. *Science* **2019**, *365*, 159–161.

DOI: 10.31635/ccschem.021.202100789
Corrected Citation: *CCS Chem.* **2022**, 4, 1016–1027
Previous Citation: *CCS Chem.* **2021**, 3, 1115–1126
Link to VoR: https://doi.org/10.31635/ccschem.021.202100789

3. Tromans, R. A.; Carter, T. S.; Chabanne, L.; Crump, M. P.; Li, H.; Matlock, J. V.; Orchard, M. G.; Davis, A. P. A Biomimetic Receptor for Glucose. *Nat. Chem.* **2019**, *11*, 52–56.
4. Liu, M.; Zhang, L.; Little, M. A.; Kapil, V.; Ceriotti, M.; Yang, S.; Ding, L.; Holden, D. L.; Balderas-Xicohténcatl, R.; He, D.; Clowes, R.; Chong, S. Y.; Schütz, G.; Chen, L.; Hirscher, M.; Cooper, A. I. Barely Porous Organic Cages for Hydrogen Isotope Separation. *Science* **2019**, *366*, 613–620.
5. Sun, N.; Wang, C.; Wang, H.; Yang, L.; Jin, P.; Zhang, W.; Jiang, J. Multifunctional Tubular Organic Cage-Supported Ultrafine Palladium Nanoparticles for Sequential Catalysis. *Angew. Chem. Int. Ed.* **2019**, *58*, 18011–18016.
6. Gosselin, E. J.; Rowland, C. A.; Bloch, E. D. Permanently Microporous Metal-Organic Polyhedra. *Chem. Rev.* **2020**, *120*, 8987–9014.
7. Chen, L.; Chen, Q. H.; Wu, M. Y.; Jiang, F. L.; Hong, M. C. Controllable Coordination-Driven Self-Assembly: From Discrete Metallocages to Infinite Cage-Based Frameworks. *Acc. Chem. Res.* **2015**, *48*, 201–210.
8. Cai, L.-X.; Li, S.-C.; Yan, D.-N.; Zhou, L.-P.; Guo, F.; Sun, Q.-F. Water-Soluble Redox-Active Cage Hosting Polyoxometalates for Selective Desulfurization Catalysis. *J. Am. Chem. Soc.* **2018**, *140*, 4869–4876.
9. Wang, D.; Chen, Z. N.; Ding, Q. R.; Feng, C. C.; Wang, S. T.; Zhuang, W.; Zhang, L. Rational Preparation of Atomically Precise Non-Alkyl Tin-Oxo Clusters with Theoretical to Experimental Insights into Electrocatalytic CO_2 Reduction Applications. *CCS Chem.* **2020**, *2*, 2607–2616.
10. Sun, L. J.; Fan, Y. L.; Yin, M. J.; Zhang, H. P.; Feng, H.; Guo, L. J.; Luo, F. Thorium Metal-Organic Framework Showing Proton Transformation from $[NH_2(CH_3)_2]^+$ to the Carboxyl Group to Enhance Porosity for Selective Adsorption of D_2 over H_2 and Ammonia Capture. *Cryst. Growth Des.* **2020**, *20*, 3605–3610.
11. Schneider, M. W.; Oppel, I. M.; Griffin, A.; Mastalerz, M. Post-Modification of the Interior of Porous Shape-Persistent Organic Cage Compounds. *Angew. Chem. Int. Ed.* **2013**, *52*, 3611–3615.
12. Sholl, D. S.; Lively, R. P. Seven Chemical Separations to Change the World. *Nature* **2016**, *532*, 435–437.
13. Li, R.-B.; Xiang, S.; Xing, H.; Zhou, W.; Chen, B. Exploration of Porous Metal-Organic Frameworks for Gas Separation and Purification. *Coord. Chem. Rev.* **2019**, *378*, 87–103.
14. Cui, X.; Chen, K.; Xing, H.; Yang, Q.; Krishna, R.; Bao, Z.; Wu, H.; Zhou, W.; Dong, X.; Han, Y.; Li, B.; Ren, Q.; Zaworotko, M. J.; Chen, B. Pore Chemistry and Size Control in Hybrid Porous Materials for Acetylene Capture from Ethylene. *Science* **2016**, *353*, 141–144.
15. Yang, S.; Ramirez-Cuesta, A. J.; Newby, R.; Garcia-Sakai, V.; Manuel, P.; Callear, S. K.; Campbell, S. I.; Tang, C. C.; Schröer, M. Supramolecular Binding and Separation of Hydrocarbons within a Functionalized Porous Metal-Organic Framework. *Nat. Chem.* **2014**, *7*, 121–129.
16. Liao, P.-Q.; Zhang, W.-X.; Zhang, J.-P.; Chen, X.-M. Efficient Purification of Ethene by an Ethane Trapping Metal-Organic Framework. *Nat. Commun.* **2015**, *6*, 8697.
17. Banerjee, D.; Simon, C. M.; Elsaidi, S. K.; Haranczyk, M.; Thallapally, P. K. Xenon Gas Separation and Storage Using Metal-Organic Frameworks. *Chem* **2018**, *4*, 466–494.
18. Zhang, H. P.; Fan, Y. L.; Krishna, R.; Feng, X. F.; Wang, L.; Luo, F. Robust Metal-Organic Framework with Multiple Traps for Trace Xe/Kr Separation. *Sci. Bull.* **2021**.
19. Cui, W.-G.; Hu, T.-L.; Bu, X.-H. Metal-Organic Framework Materials for the Separation and Purification of Light Hydrocarbons. *Adv. Mater.* **2019**, *31*, 1806445.
20. Chen, K.-J.; Madden, D. G.; Mukherjee, S.; Pham, T.; Forrest, K. A.; Kumar, A.; Space, B.; Kong, J.; Zhang, Q.-Y.; Zaworotko, M. J. Synergistic Sorbent Separation for One-Step Ethylene Purification from a Four-Component Mixture. *Science* **2019**, *366*, 241–246.
21. Zeng, H.; Xie, M.; Huang, Y.-L.; Zhao, Y.; Xie, X.-J.; Bai, J.-P.; Wan, M.-Y.; Krishna, R.; Lu, W.; Li, D. Induced Fit of C_2H_2 in a Flexible MOF through Cooperative Action of Open Metal Sites. *Angew. Chem. Int. Ed.* **2019**, *58*, 8515–8519.
22. Ding, Q.; Zhang, Z. Q.; Yu, C.; Zhang, P. X.; Wang, J.; Cui, X. L.; He, C. H.; Deng, S. G.; Xing, H. B. Exploiting Equilibrium-Kinetic Synergetic Effect for Separation of Ethylene and Ethane in a Microporous Metal-Organic Framework. *Sci. Adv.* **2020**, *6*, eaaz4322.
23. Peng, Y. L.; Pham, T.; Li, P. F.; Wang, T.; Chen, Y.; Chen, K. J.; Forrest, K. A.; Space, B.; Cheng, P.; Zaworotko, M. J.; Zhang, Z. J. Robust Ultramicroporous Metal-Organic Frameworks with Benchmark Affinity for Acetylene. *Angew. Chem. Int. Ed.* **2018**, *57*, 10971–10975.
24. Luo, F.; Yan, C. S.; Dang, L. L.; Krishna, R.; Zhou, W.; Wu, H.; Dong, X. L.; Han, Y.; Hu, T. L.; O'Keeffe, M.; Wang, L. L.; Luo, M. B.; Lin, R. B.; Chen, B. L. UTSA-74: A MOF-74 Isomer with Two Accessible Binding Sites per Metal Center for Highly Selective Gas Separation. *J. Am. Chem. Soc.* **2016**, *138*, 5678–5684.
25. Xu, Z. Z.; Xiong, X. H.; Xiong, J. B.; Krishna, R.; Li, L. B.; Fan, Y. L.; Luo, F.; Chen, B. L. A Robust Th-Azole Framework for Highly Efficient Purification of C_2H_4 from a $C_2H_4/C_2H_2/C_2H_6$ Mixture. *Nat. Commun.* **2020**, *11*, 3163.
26. Fan, W. D.; Wang, X.; Zhang, X. R.; Liu, X. P.; Wang, Y. T.; Kang, Z. X.; Dai, F. N.; Xu, B.; Wang, R. M.; Sun, D. F. Fine-Tuning the Pore Environment of the Microporous Cu-MOF for High Propylene Storage and Efficient Separation of Light Hydrocarbons. *ACS Cent. Sci.* **2019**, *5*, 1261–1268.
27. Zhai, Q. G.; Bu, X. H.; Zhao, X.; Li, D. S.; Feng, P. Y. Pore Space Partition in Metal-Organic Frameworks. *Acc. Chem. Res.* **2017**, *50*, 407–417.
28. Kim, J. Y.; Oh, H.; Moon, H. R. Hydrogen Isotope Separation in Confined Nanospaces: Carbons, Zeolites, Metal-Organic Frameworks, and Covalent Organic Frameworks. *Adv. Mater.* **2019**, *31*, 1805293.
29. Wang, H.; Li, J. Microporous Metal-Organic Frameworks for Adsorptive Separation of C_5–C_6 Alkane Isomers. *Acc. Chem. Res.* **2019**, *52*, 1968–1978.
30. Rae, H. K. *Separation of Hydrogen Isotopes (Symposium Series, ACS)*; American Chemical Society: Washington, D.C., **1978**; Vol. 68, pp 1–26.
31. Keyser, G. M.; McConnell, D. B.; Anyas-Weiss, N.; Kirkby, P. *Separation of Hydrogen Isotopes (ACS)*; American Chemical Society: Washington, D.C., **1978**; Vol. 68, pp 126–133.
32. Myers, R. A. *Handbook of Petroleum Refining Processes*; McGraw-Hill: New York, **2004**.

DOI: 10.31635/ccschem.021.202100789
Corrected Citation: *CCS Chem.* **2022**, 4, 1016–1027
Previous Citation: *CCS Chem.* **2021**, 3, 1115–1126
Link to VoR: https://doi.org/10.31635/ccschem.021.202100789

33. Chen, B. L.; Zhao, X. B.; Putkham, A.; Hong, K. L.; Lobkovsky, E. B.; Hurtado, E. J.; Fletcher, A. J.; Thomas, K. M. Surface Interactions and Quantum Kinetic Molecular Sieving for H_2 and D_2 Adsorption on a Mixed Metal-Organic Framework Material. *J. Am. Chem. Soc.* **2008**, *130*, 6411–6423.
34. Beenakker, J. M.; Borman, V. D.; Krylov, S. Y. Molecular Transport in Subnanometer Pores: Zero-Point Energy, Reduced Dimensionality and Quantum Sieving. *Chem. Phys. Lett.* **1995**, *232*, 379–382.
35. Zhang, L. D.; Jee, S.; Park, J.; Jung, M. J.; Wallacher, D.; Franz, A.; Lee, W.; Yoon, M. Y.; Choi, K. M.; Hirscher, M.; Oh, H. Exploiting Dynamic Opening of Apertures in a Partially Fluorinated MOF for Enhancing H_2 Desorption Temperature and Isotope Separation. *J. Am. Chem. Soc.* **2019**, *141*, 19850–19858.
36. Si, Y. N.; He, X.; Jiang, J.; Duan, Z. M.; Wang, W. J.; Yuan, D. Q. Highly Effective H_2/D_2 Separation in a Stable Cu-Based Metal-Organic Framework. *Nano Res.* **2021**, *14*, 518–525.
37. Kim, J. Y.; Zhang, L. D.; Balderas-Xicohténcatl, R.; Park, J.; Hirscher, M.; Moon, H. R.; Oh, H. Selective Hydrogen Isotope Separation *via* Breathing Transition in MIL-53(Al). *J. Am. Chem. Soc.* **2017**, *139*, 17743–17746.
38. Gao, L. G.; Zhang, R. M.; Xu, X. F.; Truhlar, D. G. Quantum Effects on H_2 Diffusion in Zeolite RHO: Inverse Kinetic Isotope Effect for Sieving. *J. Am. Chem. Soc.* **2019**, *141*, 13635–13642.
39. Kim, J. Y.; Balderas-Xicohténcatl, R.; Zhang, L. D.; Kang, S. G.; Hirscher, M.; Oh, H.; Moon, H. R. Exploiting Diffusion Barrier and Chemical Affinity of Metal-Organic Frameworks for Efficient Hydrogen Isotope Separation. *J. Am. Chem. Soc.* **2017**, *139*, 15135–15141.
40. Kim, J. Y.; Park, J.; Ha, J. S.; Jung, M. J.; Wallacher, D.; Franz, A.; Balderas-Xicohtencatl, R.; Hirscher, M.; Kang, S. G.; Park, J.; Oh, I. H.; Moon, H. R.; Oh, H. Specific Isotope-Responsive Breathing Transition in Flexible Metal-Organic Frameworks. *J. Am. Chem. Soc.* **2020**, *142*, 13278–13282.
41. Zhang, Z. Q.; Tan, B.; Wang, P. C.; Cui, X. L.; Xing, H. B. Highly Efficient Separation of Linear and Branched C_4 Isomers with a Tailor-Made Metal-Organic Framework. *AIChE J.* **2020**, *66*, e16236.
42. Peralta, D.; Chaplais, G.; Simon-Masseron, A.; Barthelet, K.; Pirngruber, G. D. Separation of C_6 Paraffins Using Zeolitic Imidazolate Frameworks: Comparison with Zeolite 5A. *Ind. Eng. Chem. Res.* **2012**, *51*, 4692–4702.
43. Herm, Z. R.; Wiers, B. M.; Mason, J. A.; van Baten, J. M.; Hudson, M. R.; Zajdel, P.; Brown, C. M.; Masciocchi, N.; Krishna, R.; Long, J. R. Separation of Hexane Isomers in a Metal-Organic Framework with Triangular Channels. *Science* **2013**, *340*, 960–964.
44. Wang, H.; Dong, X.; Lin, J.; Teat, S. J.; Jensen, S.; Cure, J.; Alexandrov, E. V.; Xia, Q.; Tan, K.; Wang, Q.; Olson, D. H.; Proserpio, D. M.; Chabal, Y. J.; Thonhauser, T.; Sun, J.; Han, Y.; Li, J. Topologically Guided Tuning of Zr-MOF Pore Structures for Highly Selective Separation of C_6 Alkane Isomers. *Nat. Commun.* **2018**, *9*, 1745.
45. Wang, H.; Dong, X.; Velasco, E.; Olson, D. H.; Han, Y.; Li, J. One-of-a-Kind: A Microporous Metal-Organic Framework Capable of Adsorptive Separation of Linear, Mono- and Di-Branched Alkane Isomers *via* Temperature- and Adsorbate-Dependent Molecular Sieving. *Energy Environ. Sci.* **2018**, *11*, 1226–1231.
46. Yu, L.; Dong, X. L.; Gong, Q. H.; Acharya, S. R.; Lin, Y. H.; Wang, H.; Han, Y.; Thonhauser, T.; Li, J. Splitting Mono- and Dibranched Alkane Isomers by a Robust Aluminum-Based Metal-Organic Framework Material with Optimal Pore Dimensions. *J. Am. Chem. Soc.* **2020**, *142*, 6925–6929.
47. Mendes, P. A. P.; Horcajada, P.; Rives, S.; Ren, H.; Rodrigues, A. E.; Devic, T.; Magnier, E.; Trens, P.; Jobic, H.; Ollivier, J.; Maurin, G.; Serre, C.; Silva, J. A. C. A Complete Separation of Hexane Isomers by a Functionalized Flexible Metal-Organic Framework. *Adv. Funct. Mater.* **2014**, *48*, 7666–7673.
48. Li, Y. S.; Bux, H.; Feldhoff, A.; Li, G. L.; Yang, W. S.; Caro, J. Controllable Synthesis of Metal-Organic Frameworks: From MOF Nanorods to Oriented MOF Membranes. *Adv. Mater.* **2010**, *22*, 3322–3326.
49. Li, Y. S.; Liang, F. Y.; Bux, H.; Feldhoff, A.; Yang, W. S.; Caro, J. Molecular Sieve Membrane: Supported Metal-Organic Framework with High Hydrogen Selectivity. *Angew. Chem. Int. Ed.* **2010**, *49*, 548–551.
50. Zhang, J. P.; Zhou, H. L.; Zhou, D. D.; Liao, P. Q.; Chen, X. M. Controlling Flexibility of Metal-Organic Frameworks. *Natl. Sci. Rev.* **2018**, *5*, 907–919.
51. O'Keeffe, M.; Peskov, M. A.; Ramsden, S. J.; Yaghi, O. M. The Reticular Chemistry Structure Resource (RCSR) Database of, and Symbols for, Crystal Nets. *Acc. Chem. Res.* **2008**, *41*, 1782–1789.
52. Assen, A. H.; Belmabkhout, Y.; Adil, K.; Bhatt, P. M.; Xue, D. X.; Jiang, H.; Eddaoudi, M. Tunable Rare Earth fcu-MOF Platform: Access to Adsorption Kinetics Driven Gas/Vapor Separations *via* Pore Size Contraction. *Angew. Chem. Int. Ed.* **2015**, *54*, 14353–14358.

DOI: 10.31635/ccschem.021.202100789
Corrected Citation: *CCS Chem.* **2022**, 4, 1016–1027
Previous Citation: *CCS Chem.* **2021**, 3, 1115–1126
Link to VoR: https://doi.org/10.31635/ccschem.021.202100789

Supporting Information

A $[Th_8Co_8]$ Nanocage-based MOF with Extremely Narrow Window but Flexible Nature Enabling Dual-Sieving Effect for both Isotope and Isomer Separation

Mengjia Yin,[a] Rajamani Krishna,[c] Wenjing Wang,[b] Daqiang Yuan,[b] Yaling Fan,[a] Xuefeng Feng,[a] Li Wang,[a] and Feng Luo[a]*

[a]School of Chemistry, Biology and Materials Science, East China University of Technology, Nanchang 330013

[b]State Key Laboratory of Structural Chemistry, Fujian Institute of Research on the Structure of Matter Chinese Academy of Sciences, Fuzhou, 350002

[c]Van 't Hoff Institute for Molecular Sciences, University of Amsterdam, Science Park 904, 1098 XH Amsterdam

Corresponding author: ecitluofeng@163.com

Experimental Section

Materials and physical measurements. All chemicals were directly purchased from innochem with no further purification. The optical images were accepted from Optec SZ810 microscope. Thermogravimetric analysis (TG) was performed by a TGA Q500 under a N_2 atmosphere from room temperature to 800 °C at a rate of 10 °C/min. The data of X-ray powder diffraction was collected on a Bruker AXSD8 Discover powder diffractometer at 40 kV/40 mA for Cu Kα (λ = 1.5406 Å) at room temperature in the range of 5-50 °(2θ) with a scan speed of 0.1 °per step. The gas adsorption isotherms were collected on a Belsorp-max. The N_2, D_2, H_2, C_2H_4, C_3H_6, n-C_4H_{10}, and *iso*-C_4H_{10} gases used in this adsorption experiment were ultrahigh-purity-grade (>99.999%). The vapour adsorption was carried out on Belsorp-max for the pure hexane isomer.

Gas adsorption and vapour adsorption measurements. Before carrying out the adsorption experiment, the samples of **ECUT-8** were firstly treated by immerging in CH_3OH for three days to make solvent exchange. Then the samples about 100 mg were degased at 150 °C under vacuum for 24 h in Belsorp-max. The BET was investigated by nitrogen adsorption at 77 K. The single-component isotherms of CO_2, C_3H_4, C_2H_6, C_3H_6, D_2, H_2, C_2H_4, C_3H_6, n-C_4H_{10}, *iso*-C_4H_{10}, and 1,3-butadiene were collected on the Belsorp-max. To maintain the experimental temperatures liquid nitrogen (77 K) and temperature-programmed water bath (273K, 298K) were used respectively. Similarly, the pure hexane isomers were used to carry out vapour adsorption test. The time-dependent adsorption profiles of CO_2 were measured on Intelligent Gravimetric Analyzer (IGA-100, HIDEN).

Adsorption kinetics. This was carried out by a batch experiments. In a typical experiment, approximate 10 mg activated adsorbent was placed a dried little glass bottle, then it was placed into a big glass bottle with 0.2 mL pure nHEX, or 3MP, or 2MP, or 22DMB, or 23 DMB solution. Then the big glass bottle was sealed and placed at certain temperature higher than the corresponding boiling temperature about 5°C for each hexane isomer. Then the samples were taken out every five seconds. The difference in weight between the activated samples and the samples after loading C_6 vapour was obtained through a 1/10000 scales.

Hexane isomer separation. Batch experiments was carried out to test the adsorption of hexane isomers in the liquid phase. In a typical experiment, 10 mg adsorbent was accurately measured and immersed in 0.25 mL equal volume mixtures such as nHEX/3MP, nHEX/2MP, nHEX/22DMB, 2MP/3MP, 2MP/22DMB, 3MP/22DMB, nHEX/3MP/2MP, nHEX/3MP/22DMB, and

nHEX/2MP/3MP/ 22DMB for 24 h at room temperature. Then, the samples were dried on filter paper for 12 hours to remove liquid from the surface of the crystals. The guest molecules were extracted with butyl acetate (1mL) overnight. Extracted liquid (0.5 mL) was analyzed by GC, and the content and purity of hexane isomers was obtained. Because GC shows few effect on the separation of 23DMB and 22DMB, thus, in this work, we just researched 22DMB.

The intracrystalline diffusivity of gas molecules in porous media.

The intracrystalline diffusivity of gas molecules in porous media is D_c,

$$\frac{m_t}{m_\infty} \approx \frac{6}{Rc}\sqrt{\frac{Dct}{\pi}} \left(m_t / m_\infty < 0.3\right) \quad (1)$$

In Eq. 1, m_t is the gas uptake at time t; m_∞ is the gas uptake at equilibrium; D_c is the intracrystalline diffusivity of gas molecules in porous media; and R_c is the radius of the equivalent spherical particle. From the slope k ($\frac{m_t}{m_\infty}$ plotted against $\sqrt{t}$), D_c can be further derived as

$$Dc = \frac{k^2 R_c^2 \pi}{36} \quad (2)$$

Breakthrough experiment for gas separation. In a typical experiment, 0.8 g activated adsorbent was added into the packed column (Ø 46 mm×150 mm). Before starting each experiment, helium reference gas is flushed through the column and then the gas flow was switched to the desired gas mixture at the setted flow rate. The gas mixture downstream the column was monitored using a Hiden mass-spectrometer.

Breakthrough experiment for liquid separation. In a typical experiment, 0.8 g activated adsorbent was added into the packed column (Ø 46 mm×150 mm). Then, 5 ml equal volume of nHEX/2MP/3MP/22DMB mixed solution was added into this column. The breaked solution was obtained every 5 second, which was futher analyzed by GC, giving the content of hexane isomers. A multicomponent breakthrough curves were obtained by plotting the change of content of each hexane isomers with time. Because GC shows few effect on the separation of 23DMB and 22DMB, thus, in this work, we just researched 22DMB.

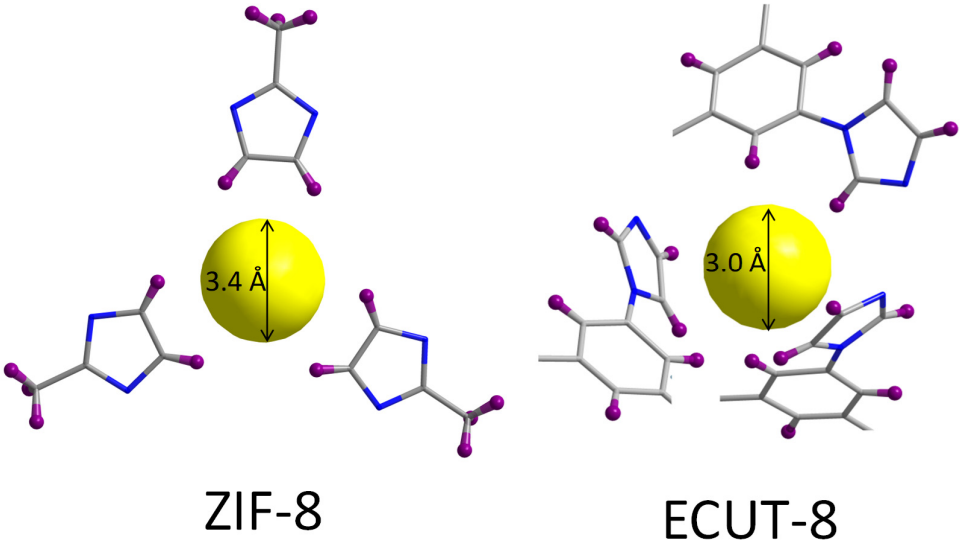

Figure S1. A comparison of the six-ring narrow window in ZIF-8 and **ECUT-8**.

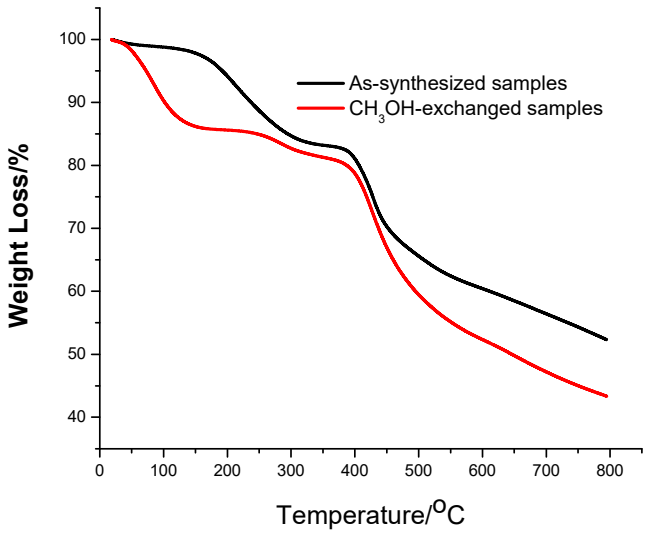

Figure S2. The TG plots of as-synthesized **ECUT-8** and the CH_3OH-exchanged samples.

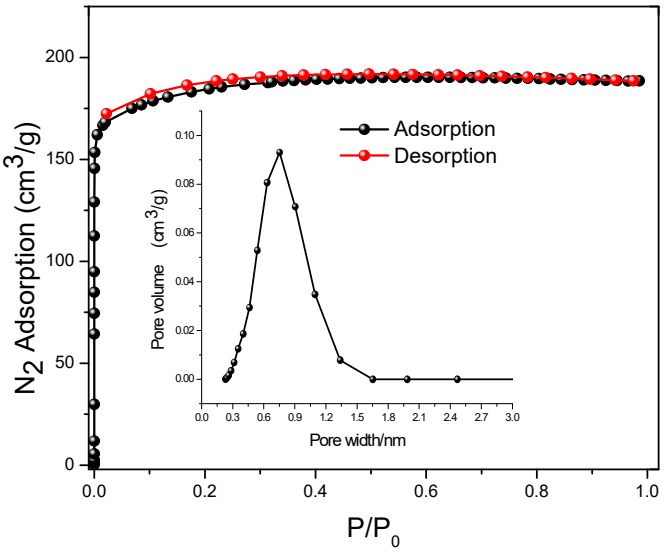

Figure S3. The N_2 adsorption at 77 K with the insert of the distribution of pore size.

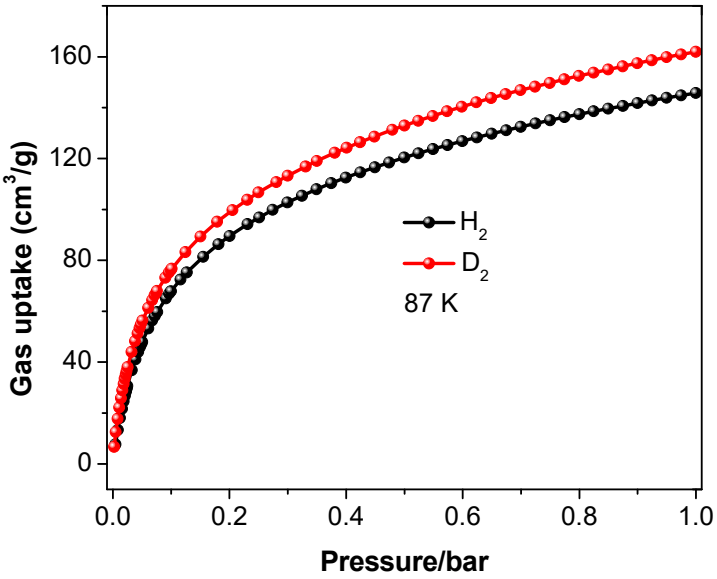

Figure S4. The H_2, D_2 adsorption isotherms at 87 K.

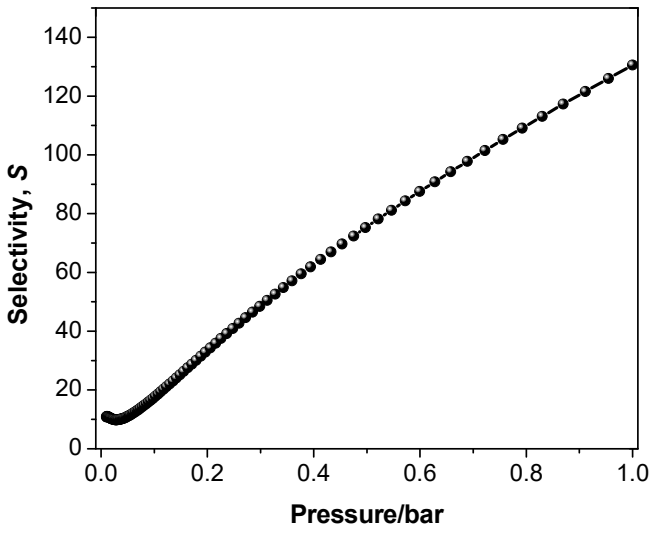

Figure S5. The n-butane/*iso*-butane selectivity at 298 K.

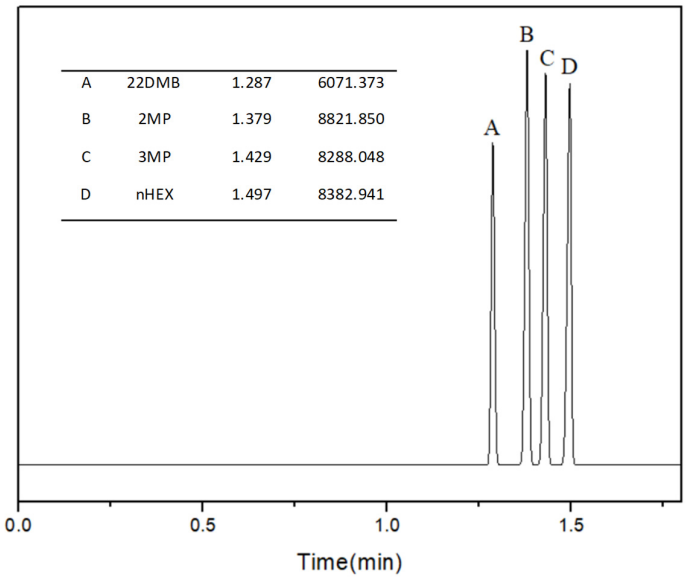

Figure S6. The GC standard peaks for the solution of nHEX, 2MP, 3MP, and 22DMB.

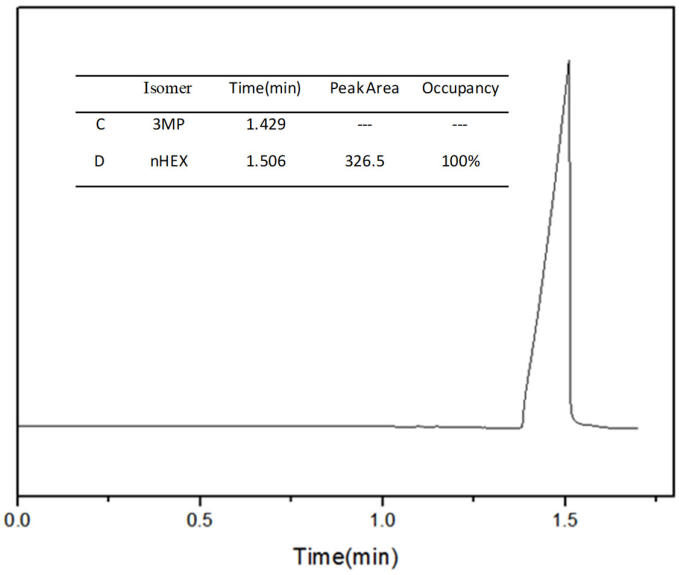

Figure S7. The GC results of the solution for nHEX/3MP separation upon activated **ECUT-8** samples.

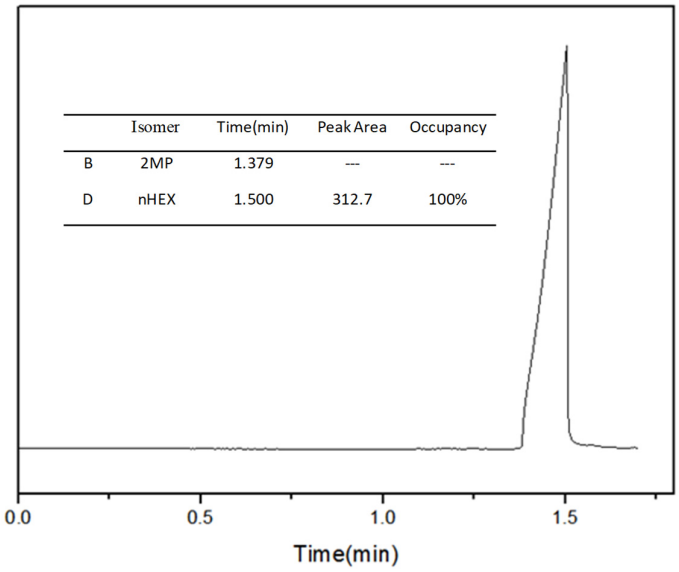

Figure S8. The GC results of the solution for nHEX/2MP separation upon activated **ECUT-8** samples.

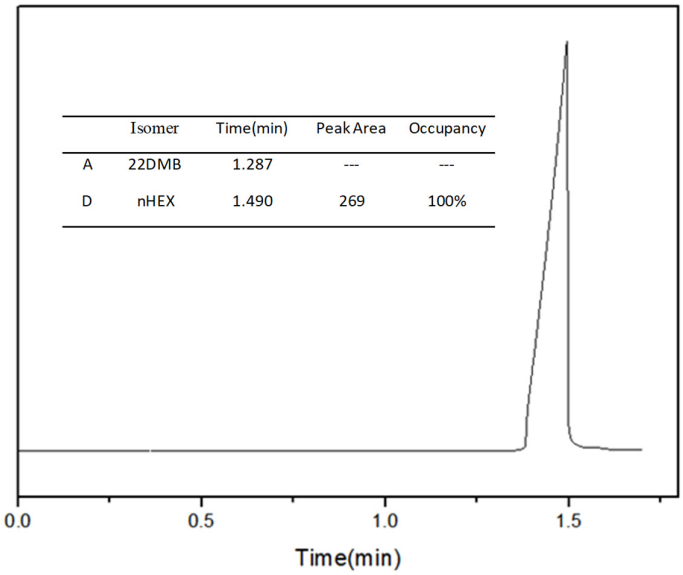

Figure S9. The GC results of the solution for nHEX/22DMB separation upon activated **ECUT-8** samples.

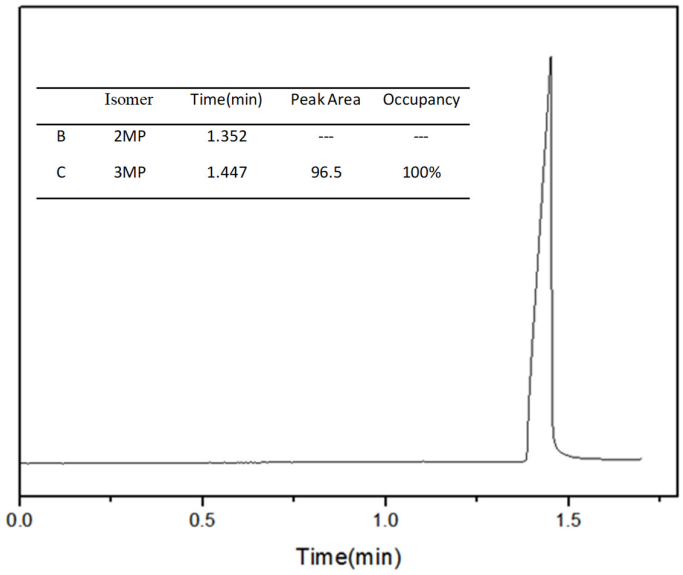

Figure S10. The GC results of the solution for 3MP/2MP separation upon activated **ECUT-8** samples.

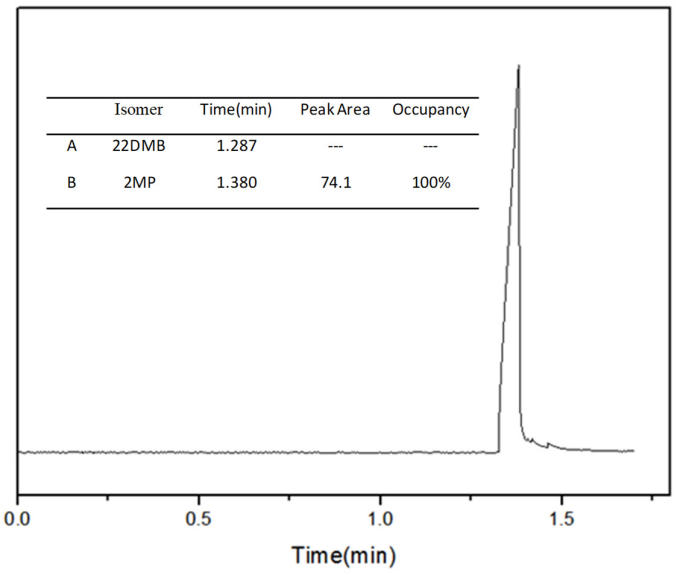

Figure S11. The GC results of the solution for 22DMB/2MP separation upon activated **ECUT-8** samples.

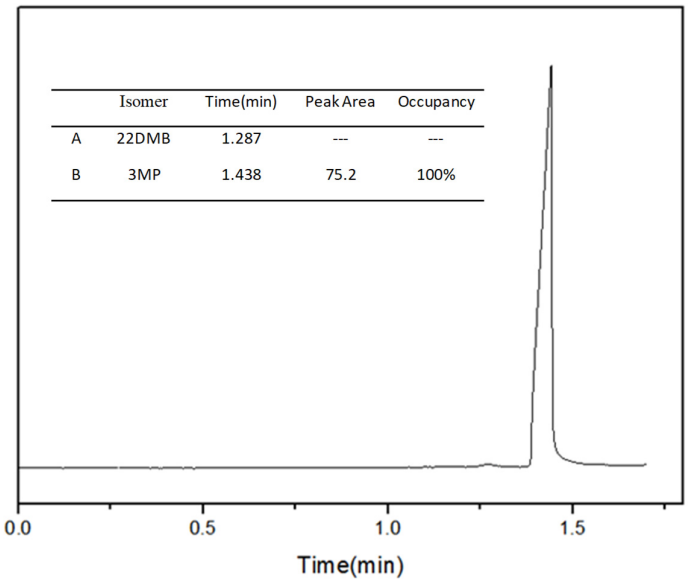

Figure S12. The GC results of the solution for 22DMB/3MP separation upon activated **ECUT-8** samples.

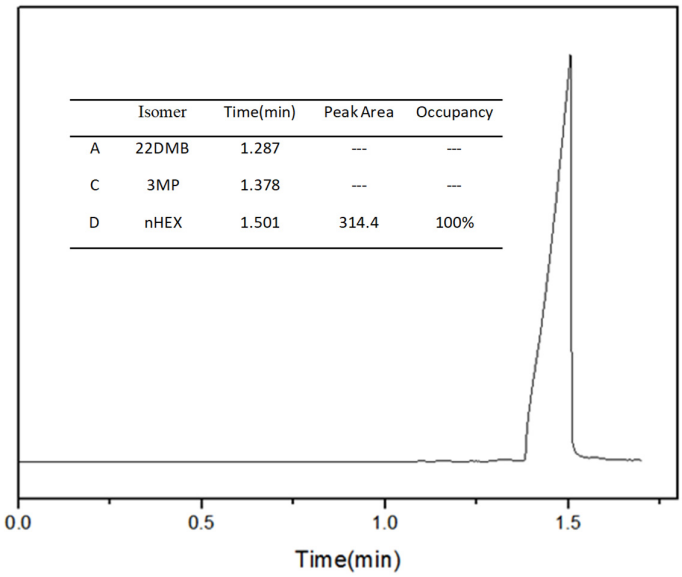

Figure S13. The GC results of the solution for nHEX/3MP/22DMB separation upon activated **ECUT-8** samples.

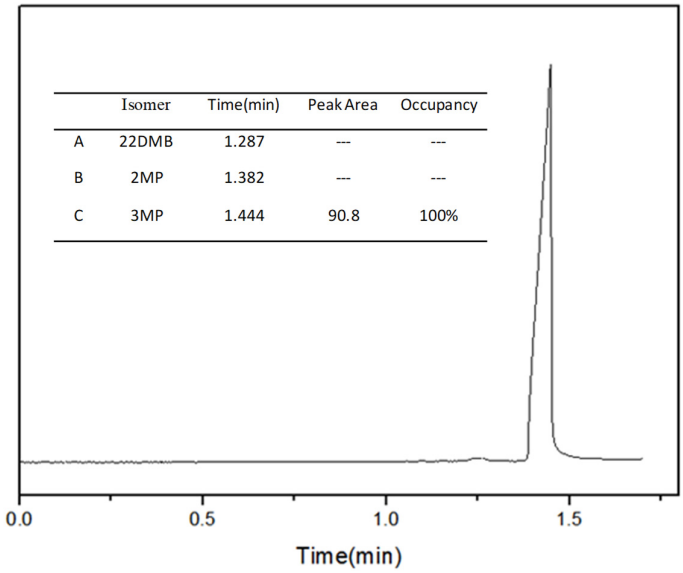

Figure S14. The GC results of the solution for 2MP/3MP/22DMB separation upon activated **ECUT-8** samples.

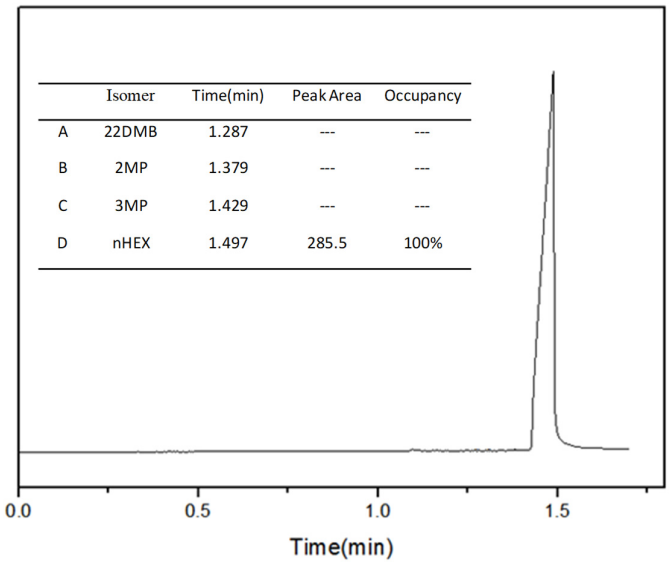

Figure S15. The GC results of the solution for nHEX/2MP/3MP/22DMB separation upon activated **ECUT-8** samples.

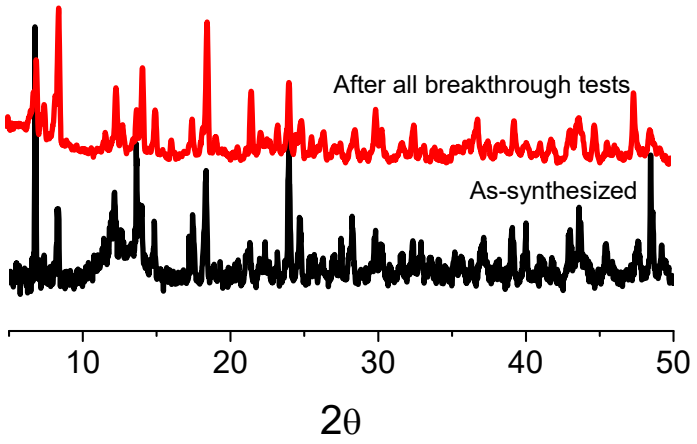

Figure S16. A comparison of PXRD patterns for the as-synthesized samples and the **ECUT-8** samples after finishing all breakthrough experiments.

Table S1. A crystallographic summarization of **ECUT-8**.

Compound	**ECUT-8**
Molecular formula	$ThCoL_3 \cdot 3$ DMF
Temperature	296 K
Crystal system	Rhombohedral
Space group	*R-3*$_2$
Unit cell, a,b,c	a=b= 14.5772(2) Å c= 38.3401(10) Å
Volume	7055.6(3) m^3
Z	6
Cell measurement reflns used	9379
F(000)	2826
Flack factor	0.5
GOF	1.127
Completion	99.9%
wR_1	0.0373
wR_2	0.1006
CCDC number	2055060